Soft Matter

PAPER

View Article Online
View Journal | View Issue

Cite this: *Soft Matter*, 2016, **12**, 6422

An insight into polymerization-induced self-assembly by dissipative particle dynamics simulation†

Feng Huang, Yisheng Lv, Liquan Wang,* Pengxiang Xu, Jiaping Lin and Shaoliang Lin*

Received 17th April 2016,
Accepted 4th July 2016

DOI: 10.1039/c6sm00912c

www.rsc.org/softmatter

Polymerization-induced self-assembly is a one-pot route to produce concentrated dispersions of block copolymer nano-objects. Herein, dissipative particle dynamics simulations with a reaction model were employed to investigate the behaviors of polymerization-induced self-assembly. The polymerization kinetics in the polymerization-induced self-assembly were analyzed by comparing with solution polymerization. It was found that the polymerization rate enhances in the initial stage and decreases in the later stage. In addition, the effects of polymerization rate, length of macromolecular initiators, and concentration on the aggregate morphologies and formation pathway were studied. The polymerization rate and the length of the macromolecular initiators are found to have a marked influence on the pathway of the aggregate formations and the final structures. Morphology diagrams were mapped correspondingly. A comparison between simulation results and experimental findings is also made and an agreement is shown. This work can enrich our knowledge about polymerization-induced self-assembly.

Introduction

Block copolymer nano-objects have attracted wide attention due to their broad applications in the fields of drug delivery, nanoreactors, biomineralizations, and so on.[1] Self-assembly is a widely accepted strategy for the construction of nano-objects with diversified morphologies including spheres, worms, vesicles, and others.[2–6] Such a strategy is based on the synthesized block copolymers and requires several necessary post-polymerization steps such as synthesis and purification before the self-assembly process.[7] In addition, traditional self-assembly is usually conducted at extremely low concentration of polymers. Therefore, the traditional self-assembly strategy encounters difficulties in the preparation of large amount of materials in scale-up industry production.

In contrast to traditional self-assembly, polymerization-induced self-assembly (PISA) can meet the demand of scale-up industry production.[8] PISA is a well-established one-pot route to produce concentrated dispersions of block copolymer nano-objects.[9] This approach relies on the use of a solvent-soluble macromolecular chain transfer agent or initiator that is polymerized with monomers to form an amphiphilic diblock copolymer in solutions.[10] Since the insolubility of the blocks increases with the block length extension during the course of polymerization, the amphiphilic diblock copolymers self-assemble into a set of polymer nano-objects.[11–17] A wide range of well-defined morphologies were produced by PISA, including spheres, worms, vesicles, concentric vesicles, large-compound vesicles and so on.[18–20] Although PISA has its inherent advantages in terms of versatility and efficiency, it is still a young field for research studies and the fundamental understanding of PISA remains incomplete in several aspects.[9,16,17,21–27] For example, the essential difference between PISA and traditional self-assembly is unclear; the physical mechanism (equilibrium or non-equilibrium behavior) underlying the balance between polymerization and self-assembly needs to be explored; and the phase diagrams in PISA should be mapped out to reproduce the PISA process. Insight into these problems can promote nano-object development from trial-and-error towards knowledge-driven innovation. Computer simulations can contribute to address these problems in a faster, effective and economic way.[28–36]

Dissipative particle dynamics (DPD) is one of the powerful computer simulation tools to study the self-assembly of block copolymers.[37–42] Recently, the method has also been developed for systems containing chemical reactions.[43–47] Lu *et al.* employed a reasonable physical reaction model to investigate surface-initiated polymerization within the DPD framework.[48] The reaction is taken as a probability issue to judge whether the reaction can take place or not. By modifying initiator densities and polymerization rates, polymer brushes with various chain lengths and polydispersities

Shanghai Key Laboratory of Advanced Polymeric Materials, Key Laboratory for Ultrafine Materials of Ministry of Education, School of Materials Science and Engineering, East China University of Science and Technology, Shanghai 200237, China. E-mail: slin@ecust.edu.cn, lq_wang@ecust.edu.cn

† Electronic supplementary information (ESI) available. See DOI: 10.1039/c6sm00912c

were obtained. Noguchi *et al.* likewise employed a binding reaction model based on probability to study the polymerization of hydrophilic blocks on an oil droplet surface.[49] Shape deformation from an oil droplet into a toroidal vesicle occurs induced by chemical reactions. Due to its success in studying polymer systems combining chemical reactions and self-assembly, this developed DPD method can be used to study the behavior of PISA.

In this work, a probability-based physical reaction model within the DPD framework was employed to simulate the PISA system consisting of macromolecular initiators, monomers and selective solvents. The effects of the polymerization rate, length of macromolecular initiators and concentration on the kinetics of PISA were examined, and morphology diagrams of the nano-objects were mapped out. A comparison with traditional self-assembly was made to show how polymerization disturbs the self-assembly behavior. Moreover, the simulation results were compared with experimental observations, and an agreement was shown.

Method and model

The dissipative particle dynamics (DPD) method is a coarse-grained mesoscopic simulation technique, which is first proposed by Hoogerbrugge and Koelman in 1992.[50] Within the method, one coarse-grained DPD bead represents a group of atoms clustered together. The position and momentum are governed by Newton's equation of motion:

$$\frac{\mathrm{d}\mathbf{r}_i}{\mathrm{d}t} = \mathbf{v}_i \quad m_i\frac{\mathrm{d}\mathbf{v}_i}{\mathrm{d}t} = \mathbf{f}_i \tag{1}$$

where $\mathbf{r}_i$, $\mathbf{v}_i$, $\mathbf{f}_i$ and m_i denote the position, velocity, total force and mass of the bead i, respectively. Three addition forces are used to describe the interaction between non-bonded beads i and j: conservative force ($\mathbf{F}^{\mathrm{C}}$), dissipative force ($\mathbf{F}^{\mathrm{D}}$), and random force ($\mathbf{F}^{\mathrm{R}}$). Hence the sum of the three interactions is given by

$$\mathbf{f}_i = \sum_{j\neq i}\left(\mathbf{F}_{ij}^{\mathrm{C}} + \mathbf{F}_{ij}^{\mathrm{D}} + \mathbf{F}_{ij}^{\mathrm{R}}\right) \tag{2}$$

The conservative force is a soft repulsion for non-bonded beads and is given by

$$\mathbf{F}_{ij}^{\mathrm{C}} = a_{ij}\sqrt{\omega(r_{ij})}\hat{\mathbf{r}}_{ij} \tag{3}$$

Where a_{ij} represents the interaction parameter between beads i and j, $\mathbf{r}_{ij} = \mathbf{r}_i - \mathbf{r}_j$, $r_{ij} = |\mathbf{r}_{ij}|$, $\hat{\mathbf{r}}_{ij} = \mathbf{r}_{ij}/r_{ij}$, and $\omega(r_{ij})$ is the weight function:

$$\omega(r_{ij}) = \begin{cases} (1 - r_{ij}/r_{\mathrm{c}})^2 & (r_{ij} < r_{\mathrm{c}}) \\ 0 & (r_{ij} \geq r_{\mathrm{c}}) \end{cases} \tag{4}$$

r_{c} is the cutoff radius and is set as 1.0. The dissipative force and the random force for the thermostat in the simulation are defined as

$$\mathbf{F}_{ij}^{\mathrm{D}} = -\gamma\omega^{\mathrm{D}}(r_{ij})(\hat{\mathbf{r}}_{ij}\cdot\mathbf{v}_{ij})\hat{\mathbf{r}}_{ij} \tag{5}$$

$$\mathbf{F}_{ij}^{\mathrm{R}} = \sigma\omega^{\mathrm{R}}(r_{ij})\theta_{ij}\hat{\mathbf{r}}_{ij} \tag{6}$$

where $\mathbf{v}_{ij} = \mathbf{v}_i - \mathbf{v}_j$, γ is the friction coefficient, σ is the noise amplitude, $\omega^{\mathrm{D}}(r_{ij})$ and $\omega^{\mathrm{R}}(r_{ij})$ are weight functions for dissipative and random forces, respectively. To satisfy the fluctuation–dissipation theorem and equilibrium Gibbs–Boltzmann distribution, a certain relation needs to be fixed:

$$\omega^{\mathrm{D}}(r_{ij}) = [\omega^{\mathrm{R}}(r_{ij})]^2 = \omega(r_{ij}) \tag{7}$$

And the values of parameters γ and σ are coupled by

$$\sigma^2 = 2\gamma k_{\mathrm{B}}T \tag{8}$$

In our simulations, γ is chosen as 4.5 and $k_{\mathrm{B}}T$ is chosen as 1.0. For the copolymer system, the interaction force between bonded beads is considered to be a harmonic spring force:

$$\mathbf{F}_{ij}^{\mathrm{S}} = C(1 - r_{ij}/r_{\mathrm{eq}})\hat{\mathbf{r}}_{ij} \tag{9}$$

In this work, we choose $C = 10$ to obtain flexible chains and the equilibrium bond distance $r_{\mathrm{eq}} = 0.8$. Reduced units are adopted for all physical quantities. The units of mass, length, time, and energy are defined by m, r_{c}, τ, and $k_{\mathrm{B}}T$, respectively. The time unit τ can be formulated by

$$\tau = \sqrt{(mr_{\mathrm{c}}^2)/k_{\mathrm{B}}T} \tag{10}$$

In the work, only the chain propagation is considered while chain transfer and chain termination are omitted. We intend to simulate the general behavior of PISA systems with small rate constants of chain transfers and chain terminations. Fig. 1 shows a sketch of the bond creation process. As shown in Fig. 1, when the monomers B meet the active ends C of macromolecular initiators within the reaction radius R ($R = 0.8\ r_{\mathrm{c}}$), the nearest monomer has a chance to connect with the end C. The probability that the active end C can polymerize with the closest monomer B is defined as P_{r}.[48] In each step of the simulation, a random number is generated. If it is smaller than the value of P_{r}, the nearest monomer B is reacted with the active end C. The reaction probability P_{r} can be used as a parameter that controls the polymerization rate. After the monomer is bonded by new bonds, the atom style and character will be changed from a hydrophilic monomer to the active end C, and the original C is replaced by B. It means that the newly connected monomers turn out to be the next growth centers for further propagation of chains. For insight into the effect of polymerization rate, P_{r} is varied in the range from 0.00001 to 0.01. Without specification, P_{r} is fixed to be 0.0001.

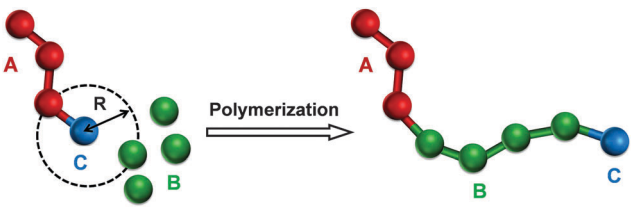

Fig. 1 A sketch of the reaction model within the DPD framework. The particles colored with red, green and blue represent hydrophilic block A, hydrophobic block B or monomer B, and active end C, respectively. Herein, a macromolecular initiator (A_3C_1) is polymerized with monomers, forming block copolymer $A_3B_4C_1$ with targeted degree of polymerization DP = 4.

In principle, the design of the probability-based reaction model is especially suitable for living free-radical polymerization.

The simulation containing a total of 81000 DPD particles was performed in a 30 × 30 × 30 cubic box under periodic boundary conditions. The density of the system was set to be 3. The repulsive interaction parameters are both simple and realistic. We took the repulsive parameter between hydrophilic block A and hydrophobic block B to be 50 (a_{AB} = 50) and that between hydrophobic block B and solvent particle S to be 75 (a_{BS} = 75). All other parameters are 25 to account for a good compatibility. Each simulation was carried out for at least 1×10^7 steps ($\Delta t = 0.04\tau$) to achieve high conversion of the monomers. Moreover, the time step for polymerization is also set to be $\Delta t = 0.04\tau$. As such, the polymerization rate is mainly decided by the value of P_r, compared with the self-assembly.

Results and discussion

In this work, we studied the polymerization kinetics and self-assembly behaviors in PISA systems containing macromolecular initiators, monomers and solvents. The effects of polymerization rate, length of macromolecular initiator, and concentrations were examined. Firstly, we focused on a special case in that A_3C_1 was used as macromolecular initiators to understand the polymerization kinetics of PISA. The targeted degree of polymerization (DP) was fixed to be 7, where the targeted DP is defined as the molar ratio of initial monomers B to macromolecular initiators. Thus, the average DP of insoluble blocks B is 7 if the monomers were completely converted in the polymerization. The total concentration of macromolecular initiators and monomers was set to be 12 vol%, and the reaction probability P_r = 0.0001. Here, the volume fraction vol% is evaluated using the ratio of total bead number of initial monomers and macromolecular initiators to that of entire systems, due to the same volume of the DPD beads.

In PISA, the self-assembly can take place as the length of insoluble B chains increases. To clarify whether self-assembly disturbs the polymerization, we also studied the solution polymerization (SP) of A_3C_1 with monomers where the B chains are soluble in the solvents (a_{BS} = 25) for a comparison. Fig. 2 shows the plots of conversion of monomers and $\ln([B]_0/[B])$ as a function of simulation time for PISA and solution polymerization. Here, $[B]_0$ and [B] are the initial monomer concentration and the monomer concentration in the polymerization, respectively. As shown in Fig. 2a, the polymerization rates for both PISA and solution polymerizations exhibit a gradual decrease with increasing time, because the monomers are consumed in both cases. Within the simulation time of $1 \times 10^6\tau$, about 98 vol% monomers are converted into the polymer chains. However, upon careful inspection of the plots of $\ln([B]_0/[B])$ *versus* time, a significant difference between PISA and solution polymerization can be observed. It can be seen that the kinetics of solution polymerizations nearly follow first-order polymerization kinetics, while the kinetics of PISA do not. At initial polymerization within the simulation time of $2 \times 10^5\tau$, the $\ln([B]_0/[B])$ of PISA is

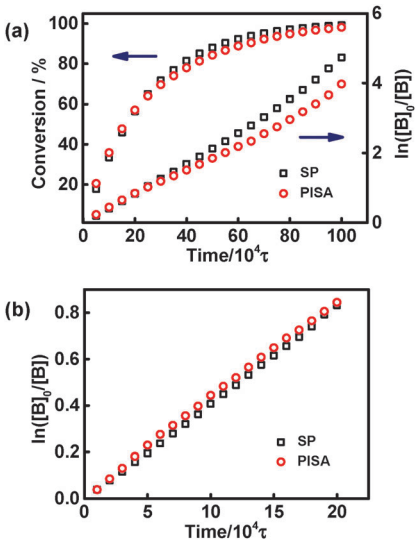

Fig. 2 (a) Conversion of monomers and $\ln([B]_0/[B])$ as a function of simulation time for PISA and solution polymerization of A_3C_1 with monomers. The total concentrations of macromolecular initiators and monomers are fixed to be 12 vol%. (b) Enlarged picture for the plots of $\ln([B]_0/[B])$ *versus* simulation time before $2 \times 10^5\tau$.

slightly larger than that of solution polymerizations, implying the polymerization rate is enhanced in PISA, as shown in Fig. 2b. This is because the monomers show a tendency to aggregate (not actually aggregate), which could increase the contact probability between monomers and active ends. As the polymerization continues, the growth of polymers in the solution polymerization always follows first-order kinetics. However, the consumption of monomers in PISA becomes slow, and the polymerization kinetics derivate from the first-order rules. This may be due to the fact that the diffusion of the monomers into the cores of the self-assemblies becomes difficult and the probability of the contact of active ends and monomers reduces as the self-assembly occurs.

Fig. 3 shows the length distribution of the block copolymer chains at various conversion stages of monomers. Here, the active ends C were not counted in the statistics, and thus the chain length of 3 corresponds to the A_3C_1 macromolecular initiators. At the conversion of 47%, about 2.8 vol% A_3C_1 macromolecular initiators were not polymerized with monomers and the induction efficiency was 97.2%. At a conversion of 81%, all macromolecular initiators were polymerized with monomers into chains and the longest chain among them was A_3B_{11}. At a conversion of 98%, the main parts of the chain constituents are 16.5 vol% A_3B_6, 15.9 vol% A_3B_7 and 16.1 vol% A_3B_8, which are in accordance with our targeted DP setting (A_3B_7). The distribution of copolymer length can be characterized by the polydispersity index (PDI), which is given by

$$\mathrm{PDI} = \frac{\bar{M}_w}{\bar{M}_n} = \frac{\sum_i N_i M_i^2 \Big/ \sum_i N_i M_i}{\sum_i N_i M_i \Big/ \sum_i N_i} \qquad (11)$$

where M is the molecule weight and N is the corresponding amount. Herein, the weight of every bead is set to be 1.0 so that

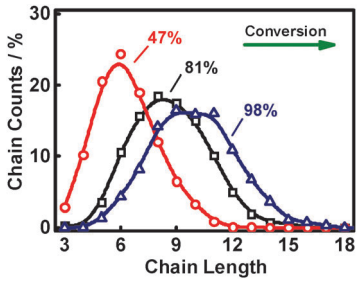

Fig. 3 Chain length distribution of block copolymer with various conversions. The active ends C are not counted in the statistics and thus the chain length of 3 corresponds to the macromolecular initiators A_3C_1.

the molecule weight is equal to the DP of chains. Through calculation, it is found that the PDI values are roughly 1.06, indicating a low polydispersity of the prepared block copolymers. Lu *et al.* employed this reaction model to investigate surface-initiated polymerization and also obtained low-polydispersity polymer brushes with a certain low reaction probability (P_r = 0.001) and initiator density.[48] The results confirmed that the probability-based model is suitable for well controlling the polymerization of PISA.

So far, we mainly consider the polymerization in PISA. In what follows, we turn to the self-assembly to get further insight into the behaviors of PISA. Fig. 4 denotes the morphology transformation during the course of PISA. The red, green, and blue colors are assigned to hydrophilic block A, hydrophobic block B and active end C, respectively. The DPD beads of solvents and monomers were omitted for clarity. As shown in Fig. 4a, at the initial homogenous stage, macromolecular initiators were dispersed freely in the solution. When the conversion reaches 31%, diblock copolymer A_3B_m with the average degree of polymerization of B blocks m = 2.2 are generated, leading to the formation of small aggregates (see Fig. 4b). With the increase in time, worm-like micelles are built upon the coalescence of neighboring aggregates, where the average DP of hydrophobic B chains increases to 3.3 (see Fig. 4c). As the polymerization continues, the worm-like micelles gradually transform into vesicles. In this transformation, the neighboring worm-like micelles first merge into a bilayer structure and bend to form bowl-like micelles (see Fig. 4d), and then close up to form vesicles (see Fig. 4e). Finally, as the conversion reaches 98%, a large-compound micelle (LCM) was observed, where the current diblock copolymers are $A_3B_{6.9}$.

To further understand the structural evolution from vesicles to LCMs, the PISA process from $6 \times 10^5\tau$ to $1 \times 10^6\tau$ was studied in detail. Fig. 5 shows the transition pathway from vesicles to LCMs, where solvent beads (orange) and the cross-section are incorporated for a clear view of vesicle cavity deformation. Blue solid objects shown in the top are solvent density graphs encapsulated in the vesicle. As can be seen from Fig. 5, the surface morphology of the vesicles remains spherical but the inner structure changes significantly. In the evolution, the inner parts pinch off and collapse at the center of the cavity. After the cavity was penetrated through, the LCM structures are formed (see Fig. 5d).

To understand how polymerization influences the self-assembly during PISA, we took the transformation from vesicles to LCMs as an example and calculated the inside solvent amounts, gyration radius R_g, and inside chain amounts for two cases. The first case is PISA with both self-assembly and polymerization, and the second case involves only the self-assembly without further polymerization. Fig. 6a shows the variation of inside solvent amounts encapsulated in the vesicles. The dotted line with the red circle and the solid line with the green triangular symbol correspond to the first and second cases, respectively. As shown in Fig. 6a, for the second case without further polymerization, the inside solvent amounts decrease rapidly. However, for the normal PISA, there is an obvious lag on the release of the solvents. At the stage from $6 \times 10^5\tau$ to $9 \times 10^5\tau$, the conversion of monomers increases from 87% to 97%, but the inside solvent amounts only decrease from 957 to 906. After that, the solvent amounts in the vesicle have a sharp decrease from 906 to 195, and finally an LCM is formed over time with only 96 solvent particles left in the micelle. This implies that the polymerization dramatically influences the self-assembly at the stage from $6 \times 10^5\tau$ to $9 \times 10^5\tau$. For the second cases without polymerization, to reach equilibrium, the vesicles quickly shrink by releasing the solvents

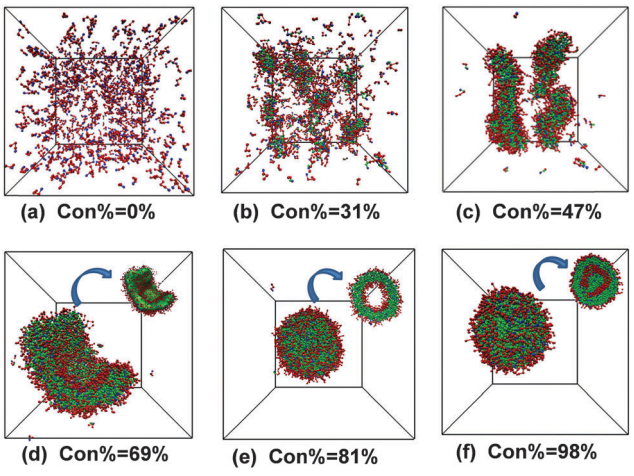

Fig. 4 Representative structures of the aggregates with various conversions during PISA. At various conversions, the average degrees of polymerization of the B chains are (a) m = 0, (b) m = 2.2, (c) m = 3.3, (d) m = 4.8, (e) m = 5.7, and (f) m = 6.9, respectively.

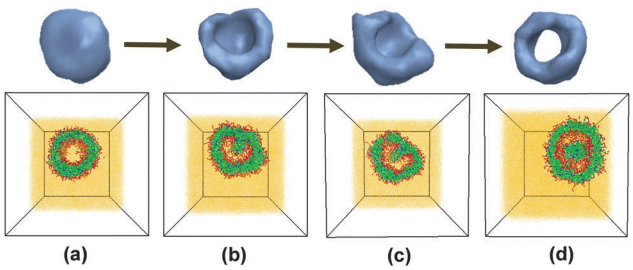

Fig. 5 Pathway for the structural evolution from vesicle to large-compound micelle during PISA. The top shows the density profiles of the encapsulated solvents in aggregates and the bottom shows the cross-section of the aggregates. The simulation times are (a) cavity integrated at $6 \times 10^5\tau$, (b) cavity pinched at $7 \times 10^5\tau$, (c) cavity collapsed at $8 \times 10^5\tau$, and (d) cavity permeated at $1 \times 10^6\tau$, respectively.

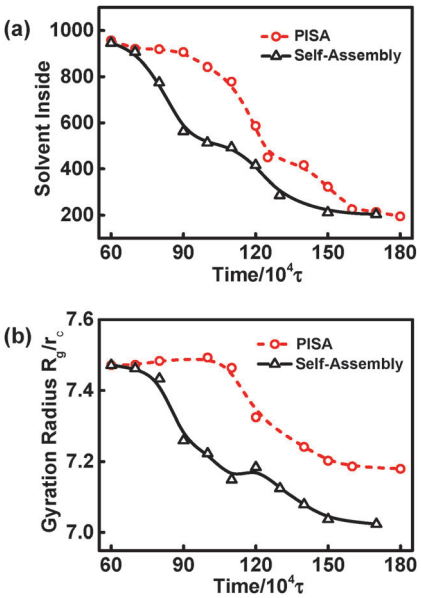

Fig. 6 (a) Variation of inside solvent amount from vesicles to large-compound micelles. Dotted line with red circles and solid line with black triangular symbols correspond to PISA and the case involving only self-assembly, respectively. (b) Variation of gyration radius R_g as a function of simulation time.

inside through the vesicular walls and transferring redundant chains on the walls to the centers to accommodate the shrinkage. While for the first case of PISA, the monomers in the solutions gradually enter into the vesicular walls and bonded to the chains *via* polymerization. Since the entrance of most of the monomers outside counteracts the release of solvents from the vesicle inside, the diffusion of solvents through vesicular walls is retarded compared with that in the second cases (note that the polymerization dominates over the release of solvents before the conversion reaches about 97% at $9 \times 10^5\tau$). This is the reason why there is a lag on the variation of the internal solvent amounts.

To characterize the shrinkage of the vesicles, the aggregate size is evaluated by gyration radius R_g, which is given by

$$R_g = \sqrt{\frac{1}{N}\sum_{i=1}^{N}(r_i - r_{cm})^2} \quad (12)$$

where r_{cm} represents the position of mass center of the aggregates and r_i represents ith position of bonded DPD beads. The variation of R_g as a function of the simulation time is presented in Fig. 6b. As shown in Fig. 6b, the R_g in the second case without further polymerization decreases dramatically. While for PISA, the vesicular size is almost unchanged at the initial stage due to the balance between chain propagation and solvent release. When the polymerization is almost completed, the vesicle shrinks dramatically, because the release of solvents dominates. Note that the aggregates obtained by PISA are larger than those in the second case, due to longer chains in the PISA. Moreover, the amount of the internal chains increases in the transition of initial stage (see Fig. S1, ESI†), suggesting that the transfer of the external chains into the center of the micelle could stabilize the structures.

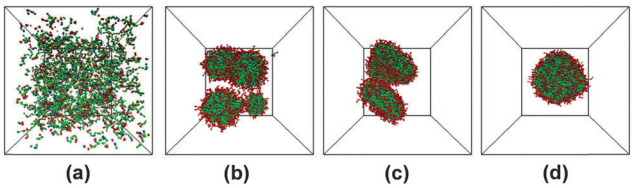

Fig. 7 Equilibrated morphology checking from traditional self-assembly for a comparison. (a) The initial solution obtained by dissolving the vesicle *via* setting repulsive parameters and running $5 \times 10^5\tau$. By turning on the primary parameter setting, self-assembled structures were obtained at various simulation times: (b) $5.5 \times 10^5\tau$, (c) $6 \times 10^5\tau$, and (d) $8 \times 10^5\tau$.

In the above comparison, the composition of the systems is changed during polymerization, leading to different pathways of self-assembly and final structures. The question arises as to whether the pathway would change if the final composition of the systems remains the same. To address this question, we carried out an additional simulation by dissolving the final aggregates obtained by PISA into diblock copolymers and then driving the diblock copolymers to self-assemble again using the same solvent conditions. When the simulation was performed, the vesicles obtained at $6 \times 10^5\tau$ were chosen to be an initial model. Then, the a_{ii} and a_{ij} values were set to be 75 (repulsive) and run for an additional $5 \times 10^5\tau$, and then the morphology can be destroyed, resulting in the free dispersion of the chains in the solvents (see Fig. 7a). Finally, the primary parameter settings are turned on to drive the self-assembly.

By tracing the time evolutions of the gyration radius, it is found that the simulated system takes only $3 \times 10^5\tau$ to reach thermodynamic equilibrium. As shown in Fig. 7b–d, in contrast with PISA, the layers are found to be not concave enough to close up to form big vesicles (see Fig. 7c). Instead of bending, the hydrophilic blocks diffuse into the center of micelles, forming large-compound micelles with irregular inner hydrophilic parts to accomplish morphology transformation.[29] The large-compound micelles should be in thermodynamic equilibrium and more stable (see Fig. S2, ESI†). The difference in the structures, *i.e.*, vesicles in PISA and large-compound micelles in traditional self-assembly, also implies that the vesicles obtained within the simulation time of $6 \times 10^5\tau$ in the PISA are out of equilibrium.

From the above two comparisons, we learned that the polymerization has a marked influence on the pathway and final structures of PISA. Therefore, polymerization rates should also exhibit a nontrivial effect on the behavior of PISA. Two typical values of P_r were set to control the polymerization rate while other conditions remained unchanged. P_r is set to be 0.01 for a faster polymerization rate, while P_r is set to be 0.00001 for a slower polymerization rate. Two different results of PISA are shown in Fig. S3 (ESI†) and Fig. 8. When P_r is 0.01, fast polymerization dominates the initial stage, and it only costs $5 \times 10^4\tau$ to achieve 100% monomer conversion (see Fig. S2, ESI†). Therefore, the latter stage is controlled by the self-assembly, and the evolution of the aggregates is similar to traditional self-assembly (see Fig. 7) with the transition from micelle "diffusion" to form LCMs (see Fig. S3b and c, ESI†). As P_r is 0.00001, the polymerization rate is not as fast as before and the conversion

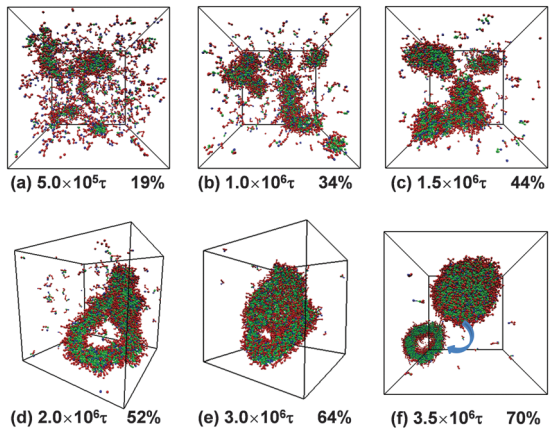

Fig. 8 Representative structures obtained in PISA with reaction probability P_r = 0.00001 at various simulation times: (a) 5 × $10^5\tau$, (b) 1 × $10^6\tau$, (c) 1.5 × $10^6\tau$, (d) 2 × $10^6\tau$, (e) 3 × $10^6\tau$, and (d) 3.5 × $10^6\tau$.

increases quite slowly, leaving sufficient time for self-assembly. As a result, the morphology transition presents a similar regularity to vesicle formation from bilayer bending and closing up (see Fig. 8). Moreover, intermediate ring-like micelles appear as the worm-like micelles transform to a bilayer through micelle fusion. Given the simulation results of slow (P_r = 0.00001), moderate (P_r = 0.0001) and fast (P_r = 0.01) polymerizations, we assume that there exists a balance between polymerization and self-assembly for constructing copolymer morphologies. Therefore, a concise method to produce desired nanostructured materials is by means of modifying the balance.

Previous studies revealed that the morphologies of the aggregates could be controlled by the length of hydrophilic blocks, the concentration of polymers, temperature, *etc.*[11] Therefore, the effects of the length of macromolecular initiators and the total concentration of macromolecular initiators and monomers on the behavior of PISA were investigated in addition to the polymerization rate. Fig. 9 shows the dynamic morphology diagram in the space of the length of macromolecular initiators *versus* the simulation time. The macromolecular initiators of A_4C_1, A_5C_1, and A_6C_1 are considered at the same reaction probability P_r = 0.0001. The system contains 880 macromolecular initiators and the targeted DP is 7 in the simulation. As such, the amounts of active ends and monomers remain unchanged in the work. Note that for each case the monomer conversion is completed within 2 × $10^6\tau$. As shown in Fig. 9, the morphology transition occurs mainly within the simulation time of 6 × $10^5\tau$. In addition, in the latter period until 2 × $10^6\tau$, the self-assembly dominates the PISA to achieve thermodynamic equilibrium of the systems. From the dynamic morphology diagram, we can see that the lengths of the macromolecular initiators have a pronounced effect on the morphology transformations. It is well known that copolymers with longer hydrophilic block length have a tendency to form stable aggregates with larger curvature in selective solvents. In the case that the length of macromolecular initiators is less than 5, morphology transformations of S → S + W → W → L → V → LCM were observed (see Fig. 4). However, when A_5C_1 or A_6C_1 is used as the initial macromolecular initiator, ring-like micelles were observed finally, while the transformation pathways to form ring-like micelles are completely different from each other.

Fig. 10 presents two different pathways of ring-like micelle formation. As shown in Fig. 10a–d, for A_5C_1 macromolecular initiators, the spherical micelles firstly coalesce into worm-like micelles, then grow into branched worm-like micelles, and finally connect to form ring-like micelles (Mechanism I). For the A_6C_1 macromolecular initiators, as shown in Fig. 10a′–d′, a different growth pathway (Mechanism II) is followed. Different from Mechanism I by close contact, this pathway goes through further evolution of LCMs. From the cross-section, it can be seen that the hydrophilic cores of the LCMs firstly gather and the morphology of the LCM transforms into an ellipse. Both the external and internal hydrophilic blocks are promptly linked to form a ring-like structure. These two typical mechanisms are in accordance with the simulation results reported by Liang *et al.*, where ring-like micelles are formed *via* two pathways including micelle coalescence and micelle growth.[51]

Fig. S4 (ESI†) shows the morphology diagram as a functional of the total initial concentration of macromolecular initiators and monomers for various targeted DPs. Each case runs for 2 × $10^6\tau$ to achieve high monomer conversion and thermodynamic equilibrium of the systems. It was found that the

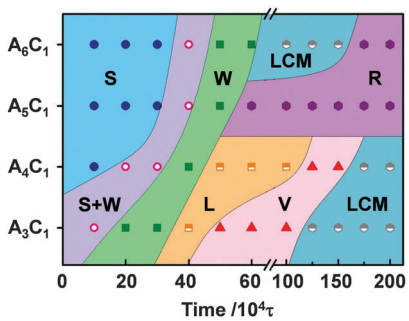

Fig. 9 Dynamic morphology diagram in space of the length of the macromolecular initiators *versus* the simulation time. The targeted block copolymers are A_mB_7 (m = 4, 5, 6). The letters S, W, L, V, LCM, and R represent spherical micelles, worm-like micelles, layer, vesicles, large-compound micelles, and ring-like micelles, respectively.

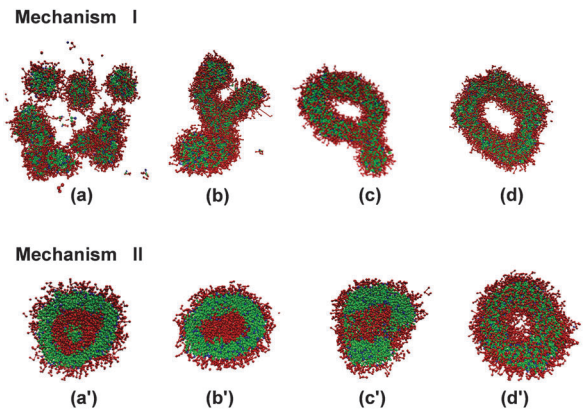

Fig. 10 Pathways of the formation of ring-like micelles for the systems containing A_5C_1 (a–d) and A_6C_1 (a′–d′).

targeted DPs have a significant impact on the morphologies of the aggregates. At a low targeted DP of 2, the polymers with short hydrophobic blocks are able to form loose aggregates, especially spherical micelles. As the targeted DP is increased to 4, more monomers would be consumed to form hydrophobic blocks. As a result, the spherical micelles coalesce to form worm-like micelles. Upon further increasing the targeted DP, the morphology changes to vesicles and then arranges to form LCMs to minimize the free energy. Note that the total initial concentration of macromolecular initiators and monomers shows less marked influence on the morphologies. However, the dimensions of the aggregates can be controlled by adjusting the concentration. For example, for the targeted A_3B_4, a single branched worm was formed at lower concentrations, while a mass of worms are clustered to form a network at higher concentrations (see Fig. 11a and b). Similarly, for targeted A_3B_8, there also exists a dimension enhancement phenomenon as the concentration increases. The calculation of the gyration radius demonstrates that the size increases with increasing of the total initial concentrations of macromolecular initiators and monomers (see Fig. S5, ESI†). This observation also holds true for the cases with higher polymerization rates (see Fig. S5, ESI†).

There are several available experimental findings for comparison. Armes *et al.* studied PISA kinetics to tackle the process of *in situ* structure evolution on PISA which utilizes poly(glycerol monomethacrylate) (PGMA) as a macromolecular initiator inducing the polymerization of 2-hydroxypropyl methacrylate (HPMA), and found a polymerization rate enhancement due to micelle aggregation.[12] In our simulation, we also found that the polymerization rate is enhanced in the initial stage. This phenomenon can be understood as follows. Since the growth of B chains and subsequently self-assembly in the process, the resulting hydrophobic B blocks would exclude solvents (a_{BS} = 75) and attract monomers (a_{BM} = 25) to lower the total surface energy, leading to a relatively high local monomer concentration, which would increase the polymerization rate. Armes *et al.* also explained that the unreacted monomers enter and solvate micelle cores, which produces a high local monomer concentration and thereby induces rate enhancement.[12] These two explanations are consistent. In addition, we also found that the polymerization rate decreases at the later stage. This is due to the following reasons. As the stable micelles are formed, the active ends are shielded in the center of the micelles and the probability to react with monomers becomes smaller, resulting in a decrease of the polymerization rate.

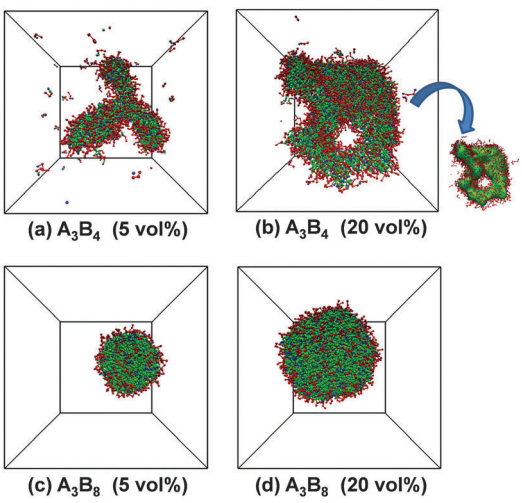

Fig. 11 Equilibrated structures formed at various total initial concentrations of macromolecular initiators and monomers: (a) 5 vol% for targeted A_3B_4, (b) 20 vol% for targeted A_3B_4, (c) 5 vol% for targeted A_3B_8, and (d) 20 vol% for targeted A_3B_8.

Pan *et al.* have investigated the morphology transition of PISA using polystyrene (PS) as a core-forming block combined with various alcohol-soluble macromolecular initiators such as poly(4-vinylpyridine) (P4VP),[20] poly(acrylic acid) (PAA)[11] and poly-(2-dimethylaminoethyl methacrylate) (PDMAEMA).[21] A continuous morphology transition from spherical micelles to worms, and finally to vesicles, was observed during the polymerization. In such a PISA system, the final structures depend on the following parameters: the polymerization conversion, the total initial concentrations of macromolecular initiators and monomers, the solvent amount, and the structure of the macromolecular initiators. In our simulation, an identical morphology transition was confirmed firstly using DPD simulation with a reaction model. We constructed the phase diagram and demonstrated the effect of polymerization rate, concentration and the macromolecular initiator structures, which are consistent with experimental findings.

Conclusions

In this work, a dissipative particle dynamics (DPD) simulation was utilized to investigate the behaviors of polymerization-induced self-assembly (PISA). A probability-based bond creation model was constructed in the framework of DPD, and it was demonstrated that a good control of the polymerization could be achieved in the simulation. The polymerization rates in the PISA were found to derivate from first-order rules, where the rate enhances in the initial stage and decreases in the later stage. Under the process of polymerization and self-assembly, various morphologies of the aggregates were observed, including spheres, worms, vesicles, large-compound micelles, and so on. Continuous morphology transformations driven by the propagation of the hydrophobic chain were observed to be consistent with experimental findings. By comparison with traditional self-assembly in selective solvents, PISA undergoes a different pathway in terms of the balance between polymerization and self-assembly. By adjusting the polymerization probabilities, the balance can be modified and diverse morphologies can be obtained. In addition, the length of the macromolecular initiators was proved to have an important role in determining the PISA process, and the concentration shows an effect on the size of the aggregates. Morphology diagrams were mapped out in the space of the length of the macromolecular initiators *versus* the simulation time and in the space of the targeted DP *versus* concentration. The simulation results were finally compared with the available experimental observations, and some consistence was shown. This work could be useful to comprehend the behaviors of polymerization-induced self-assembly.

Acknowledgements

This work was supported by the National Natural Science Foundation of China (51573046, 51103044, and 21304035). Support from the Projects of Shanghai Municipality (14SG29) and the Fundamental Research Funds for the Central Universities (NCET-12-0857, B14018 and WD1213002) is also appreciated.

References

1 Y. Mai and A. Eisenberg, *Chem. Soc. Rev.*, 2012, **41**, 5969–5985.
2 H. Qiu, Z. M. Hudson, M. A. Winnik and I. Manners, *Science*, 2015, **347**, 1329–1332.
3 J. Wang, Y. Ni, W. Jiang, H. Li, Y. Liu, S. Lin, Y. Zhou and D. Yan, *Small*, 2015, **11**, 4485–4490.
4 Y. Wang, S. Lin, M. Zang, Y. Xing, X. He, J. Lin and T. Chen, *Soft Matter*, 2012, **8**, 3131–3138.
5 D. E. Discher and A. Eisenberg, *Science*, 2002, **297**, 967–973.
6 C. Cai, J. Lin, X. Zhu, S. Gong, X.-S. Wang and L. Wang, *Macromolecules*, 2016, **49**, 15–22.
7 S. Lin, Y. Wang, C. Cai, Y. Xing, J. Lin, T. Chen and X. He, *Nanotechnology*, 2013, **24**, 085602.
8 W. Wan, X. Sun and C. Pan, *Macromolecules*, 2009, **42**, 4950–4952.
9 N. J. Warren and S. P. Armes, *J. Am. Chem. Soc.*, 2014, **136**, 10174–10185.
10 D. Zehm, L. P. D. Ratcliffe and S. P. Armes, *Macromolecules*, 2012, **46**, 128–139.
11 W. He, X. Sun, W. Wan and C. Pan, *Macromolecules*, 2011, **44**, 3358–3365.
12 A. Blanazs, J. Madsen, G. Battaglia, A. J. Ryan and S. P. Armes, *J. Am. Chem. Soc.*, 2011, **133**, 16581–16587.
13 A. Blanazs, A. J. Ryan and S. P. Armes, *Macromolecules*, 2012, **45**, 5099–5107.
14 I. Chaduc, A. s. Crepet, O. Boyron, B. Charleux, F. D'Agosto and M. Lansalot, *Macromolecules*, 2013, **46**, 6013–6023.
15 S. L. Canning, G. N. Smith and S. P. Armes, *Macromolecules*, 2016, **49**, 1985–2001.
16 Y. Su, X. Xiao, S. Li, M. Dan, X. Wang and W. Zhang, *Polym. Chem.*, 2014, **5**, 578–587.
17 Z. Ding, C. Gao, S. Wang, H. Liu and W. Zhang, *Polym. Chem.*, 2015, **6**, 8003–8011.
18 J. Sun, C. Hong and C. Pan, *Soft Matter*, 2012, **8**, 7753–7767.
19 G. Delaittre, J. Nicolas, C. Lefay, M. Save and B. Charleux, *Soft Matter*, 2006, **2**, 223–231.
20 W. Zhang, C. Hong and C. Pan, *Macromolecules*, 2014, **47**, 1664–1671.
21 W. Cai, W. Wan, C. Hong, C. Huang and C. Pan, *Soft Matter*, 2010, **6**, 5554–5561.
22 W. Zhao, G. Gody, S. Dong, P. B. Zetterlund and S. Perrier, *Polym. Chem.*, 2014, **5**, 6990–7003.
23 N. J. Warren, O. O. Mykhaylyk, A. J. Ryan, M. Williams, T. Doussineau, P. Dugourd, R. Antoine, G. Portale and S. P. Armes, *J. Am. Chem. Soc.*, 2015, **137**, 1929–1937.
24 N. J. Warren, O. O. Mykhaylyk, D. Mahmood, A. J. Ryan and S. P. Armes, *J. Am. Chem. Soc.*, 2014, **136**, 1023–1033.
25 C. Gonzato, M. Semsarilar, E. R. Jones, F. Li, G. J. P. Krooshof, P. Wyman, O. O. Mykhaylyk, R. Tuinier and S. P. Armes, *J. Am. Chem. Soc.*, 2014, **136**, 11100–11106.
26 J. Tan, Y. Bai, X. Zhang and L. Zhang, *Polym. Chem.*, 2016, **7**, 2372–2380.
27 E. R. Jones, M. Semsarilar, P. Wyman, M. Boerakker and S. P. Armes, *Polym. Chem.*, 2015, **17**, 835–857.
28 S. Lin, X. He, Y. Li, J. Lin and T. Nose, *J. Phys. Chem. B*, 2009, **113**, 13926–13934.
29 M. Xiao, G. Xia, R. Wang and D. Xie, *Soft Matter*, 2012, **8**, 7865–7874.
30 X. Li, M. Deng, Y. Liu and H. Liang, *J. Phys. Chem. B*, 2008, **112**, 14762–14765.
31 Y. Han, H. Yu, H. Du and W. Jiang, *J. Am. Chem. Soc.*, 2009, **132**, 1144–1150.
32 S. Lin, N. Numasawa, T. Nose and J. Lin, *Macromolecules*, 2007, **40**, 1684–1692.
33 Z. Wu, Q. Cui and A. Yethiraj, *J. Phys. Chem. B*, 2013, **117**, 12145–12156.
34 A.-C. Shi and B. Li, *Soft Matter*, 2013, **9**, 1398–1413.
35 Y. Lin, H. Chang, Y. Sheng and H. Tsao, *Soft Matter*, 2013, **9**, 4802–4814.
36 S. Chou, H. Tsao and Y. Sheng, *J. Chem. Phys.*, 2011, **134**, 123–127.
37 L. Zhang, B. Xu and X. Wang, *J. Phys. Chem. B*, 2016, **120**, 957–964.
38 Y. Wang, B. Li, Y. Zhou, Z. Lu and D. Yan, *Soft Matter*, 2013, **9**, 3293–3304.
39 T. Jiang, L. Wang, S. Lin, J. Lin and Y. Li, *Langmuir*, 2011, **27**, 6440–6448.
40 J. Huang, Z. Fan and Z. Ma, *J. Chem. Phys.*, 2013, **139**, 064905.
41 X. Cao, L. Zhang, J. Gu, L. Wang and J. Lin, *Polymer*, 2015, **72**, 10–20.
42 X. Zhang, J. Lin, L. Wang, L. Zhang, J. Lin and L. Gao, *Polymer*, 2015, **78**, 69–80.
43 H. Liu, H. Li and Z. Lu, *Procedia Comput. Sci.*, 2011, **4**, 1021–1028.
44 X. Yong, O. Kuksenok, K. Matyjaszewski and A. C. Balazs, *Nano Lett.*, 2013, **13**, 6269–6274.
45 S. TurgmanCohen and J. Genzer, *Macromolecules*, 2012, **45**, 2128–2137.
46 X. Yong, O. Kuksenok and A. C. Balazs, *Polymer*, 2015, **72**, 217–225.
47 A. Singh, O. Kuksenok, J. Johnson and A. C. Balazs, *Polym. Chem.*, 2016, **7**, 2955–2964.
48 H. Liu, M. Li, Z. Lu, Z. Zhang and C. Sun, *Macromolecules*, 2009, **42**, 2863–2872.
49 K. M. Nakagawa and H. Noguchi, *Soft Matter*, 2015, **11**, 1403–1411.
50 P. J. Hoogerbrugge and J. M. V. A. Koelman, *Europhys. Lett.*, 1992, **19**, 155–160.
51 P. He, X. Li, M. Deng, T. Chen and H. Liang, *Soft Matter*, 2010, **6**, 1539–1546.